Biology of Reproduction, 2017, 97(3), 466–477
doi:10.1093/biolre/iox101
Research Article
Advance Access Publication Date: 28 August 2017

Research Article

Adrenomedullin improves fertility and promotes pinopodes and cell junctions in the peri-implantation endometrium†

Brooke C. Matson[1], Stephanie L. Pierce[1], Scott T. Espenschied[1], Eric Holle[2], Imani H. Sweatt[1], Eric S. Davis[1,3], Robert Tarran[1,3], Steven L. Young[1,4], Trudy A. Kohout[5], Marcel van Duin[5] and Kathleen M. Caron[1,6,*]

[1]Department of Cell Biology and Physiology, University of North Carolina at Chapel Hill, Chapel Hill, North Carolina, USA; [2]Animal Models Core Facility, University of North Carolina at Chapel Hill, Chapel Hill, North Carolina, USA; [3]Cystic Fibrosis Center/Marsico Lung Institute, University of North Carolina at Chapel Hill, Chapel Hill, North Carolina, USA; [4]Division of Reproductive Endocrinology and Infertility, Department of Obstetrics and Gynecology, University of North Carolina at Chapel Hill, Chapel Hill, North Carolina, USA; [5]Ferring Research Institute Inc., San Diego, California, USA and [6]Department of Genetics, University of North Carolina at Chapel Hill, Chapel Hill, North Carolina, USA

*__Correspondence:__ Department of Cell Biology and Physiology, University of North Carolina at Chapel Hill, 111 Mason Farm Road, CB #7545, Chapel Hill, NC 27599, USA. Tel: +919 966–5193; Fax: +919 966–6927; E-mail: kathleen_caron@med.unc.edu

†__Grant support:__ This work was supported by U.S. National Institutes of Health Grants R01 HD060860 (to KMC), R01 HD067721 (to SLY), and F30 HD085652 (to BCM) and by Ferring Research Institute Inc.
__Conference presentation:__ Presented in part at the 48th Annual Meeting of the Society for the Study of Reproduction, 18–22 June 2015, San Juan, Puerto Rico; at the Greenwald Symposium, September 2016, Kansas City, Kansas; and at the Society for Reproductive Investigation meeting, March 2017, Orlando, Florida.

Received 21 April 2017; Revised 3 August 2017; Accepted 24 August 2017

Abstract

Implantation is a complex event demanding contributions from both embryo and endometrium. Despite advances in assisted reproduction, endometrial receptivity defects persist as a barrier to successful implantation in women with infertility. We previously demonstrated that maternal haploinsufficiency for the endocrine peptide adrenomedullin (AM) in mice confers a subfertility phenotype characterized by defective uterine receptivity and sparse epithelial pinopode coverage. The strong link between AM and implantation suggested the compelling hypothesis that administration of AM prior to implantation may improve fertility, protect against pregnancy complications, and ultimately lead to better maternal and fetal outcomes. Here, we demonstrate that intrauterine delivery of AM prior to blastocyst transfer improves the embryo implantation rate and spacing within the uterus. We then use genetic decrease-of-function and pharmacologic gain-of-function mouse models to identify potential mechanisms by which AM confers enhanced implantation success. In epithelium, we find that AM accelerates the kinetics of pinopode formation and water transport and that, in stroma, AM promotes connexin 43 expression, gap junction communication, and barrier integrity of the primary decidual zone. Ultimately, our findings advance our understanding of the contributions of AM to uterine receptivity and suggest potential broad use for AM as therapy to encourage healthy embryo implantation, for example, in combination with in vitro fertilization.

Summary Sentence

Intrauterine administration of the endocrine peptide adrenomedullin promotes pinopode formation and cell junctions in the peri-implantation endometrium, bolstering fertility after blastocyst transfer in mice.

Key words: assisted reproductive technology, decidua, endometrium, fertility, implantation, in vitro fertilization (IVF), mechanisms of hormone action, pregnancy, uterus.

Introduction

Blastocyst or embryo implantation is essential for the establishment of pregnancy and occurs during the window of implantation between embryonic days (e) 3.5 and 4.5 in mice and between days 6 and 12 postfertilization in humans [1]. While embryo implantation takes place during the very early days of pregnancy, errors occurring during this process can program clinical complications of pregnancy that present later in gestation, leading to adverse maternal and fetal outcomes [2]. A complex dialog between the embryo and the endometrium coordinates this delicate and precisely timed event, offering two angles from which to approach the clinical problem of infertility, which affects millions of women and families across the world [3,4]. Modern assisted reproductive technology (ART) can address embryonic defects preventing implantation and the establishment of pregnancy by screening embryos for aneuploidy. However, in women, only about half of the euploid blastocysts transferred to the endometrial cavity in an optimally prepared uterus result in a successful pregnancy, underlining the inability of current medical techniques to alter endometrial receptivity and the need for development of improved therapies [5].

Both the embryo and the uterus express cell surface molecules that enable their physical interaction, facilitating apposition and attachment of the blastocyst to the uterine luminal epithelium. Following closure of the epithelium around the embryo, embryonic trophoblast cells breach this layer by entosing living epithelial cells [6]. While the luminal epithelium is the first cell type that comes into direct contact with the embryo, uterine stromal cells also play a large role during the peri-implantation period. Stromal cells surrounding the implantation crypt undergo a progesterone-driven differentiation process termed decidualization that enables these cells to provide support to the embryo prior to the development of a placenta [7]. A subpopulation of decidualized stromal cells adjacent to the embryo coordinate the formation of a transient, avascular region called the primary decidual zone (PDZ), which has been hypothesized to form a highly selective barrier that protects the embryo from immunological attack [8]. Despite advances in our understanding of these peri-implantation events in recent years, there is still much to be discovered about the molecular mechanisms underlying uterine receptivity and implantation.

Previously, we and others established the peptide hormone adrenomedullin (*Adm* gene, AM protein) as an endocrine factor derived from both the mother and the fetus that is important for implantation, placentation, and the overall health of a pregnancy [9,10]. Notably, female mice heterozygous for *Adm* display a subfertility phenotype, demonstrating decreased pregnancy success and decreased epithelial pinopode coverage [11,12]. Litters of $Adm^{+/-}$ dams demonstrate irregular embryonic spacing and crowding in utero as well as fetal growth restriction and loss, yielding smaller litter sizes at weaning [12]. However, the cellular and molecular pathways downstream of AM peptide in the uterus remain to be elucidated.

During the peri-implantation period, *Adm* is spatiotemporally co-expressed with components of adherens junctions, tight junctions, and gap junctions in luminal epithelium and in decidualized stroma [11,13–15]. Notably, aberrant junctional protein expression and localization in these compartments can cause problems during implantation and decidualization with implications for fertility. For example, conditional deletion of several different transcription factors alters uterine receptivity by interfering with expression of the tight junction protein claudin-1 (*Cldn1* gene, CLDN1 protein) [16–18]. Furthermore, decreased connexin 43 (*Gja1* gene, Cx43 protein) function via a dominant loss-of-function mutation or administration of a pharmacological inhibitor interferes with early implantation events, specifically decidualization and early placental angiogenesis with consequences for fetal health [19,20].

Given the spatiotemporal co-expression of *Adm* and cell junction proteins in the uterus during peri-implantation, AM may promote cell- and tissue-level organization by affecting junctional proteins. For example, in vitro studies on lymphatic endothelium previously demonstrated that AM induces organization of VE-cadherin and ZO-1 [21]. We also found that AM promotes Cx43 mRNA and protein expression; Cx43 plasma membrane linearization; and gap junction coupling and intercellular communication, all in lymphatic endothelial cells [22]. By extension, this precedent for an AM effect on cell junctions may also apply to other cell types, which we evaluate in this current study. When taken together, the subfertility phenotype of $Adm^{+/-}$ dams and evidence for AM–cell junction interactions suggest the compelling hypothesis that AM promotes cell junction integrity in epithelial and stromal cells of the uterus, supporting the early embryo during an active time of complex tissue remodeling and thereby bolstering fertility. Here, we test this hypothesis and demonstrate that AM improves implantation success and spacing in mice and promotes cell junction organization in the peri-implantation uterine epithelium and stroma.

Materials and methods

Animals

Mice with a deletion of the *Adm* gene were previously described and were maintained as a heterozygote colony on an isogenic 129S6/SvEv background [23]. Genotyping was performed using three primers: primer 1: 5′-CAGTGAGGAATGCTAGCCTC-3′; primer 2: 5′-GCTTCCTCTTGCAAAACCACA-3′; primer 3: 5′-TCGAGCTTCCAAGGAAGACCAGG-3′. Primers 1 and 3 amplify the wild-type allele (1.8 kb), while primers 2 and 3 amplify the targeted allele (1.3 kb). All animal experiments were approved by the University of North Carolina at Chapel Hill Institutional Animal Care and Use Committee.

Blastocyst transfer

Wild-type CD1 female mice at least 8 weeks old (Charles River) were mated with vasectomized CD1 IGS males (Charles River) to

generate pseudopregnant females. The morning of the vaginal plug was designated pseudopregnant day 0.5. On pseudopregnant day 2.5, e3.5 blastocysts were collected from superovulated C57BL/6 donor females (Envigo). Immediately prior to blastocyst transfer, 0.9% NaCl or 150 pmol AM (4.3 μl) (Phoenix Pharmaceuticals) was injected directly into each horn of the uterus of pseudopregnant females anesthetized with tribromoethanol (0.4 mg/g body weight). AM was co-injected with AM(24–50) (6.15 μl total) (Phoenix Pharmaceuticals) at a 20:1 AM(24–50):AM molar ratio or with complement factor H (CFH) (5.73 μl total) (R&D Systems) at a 3.3:1 CFH:AM weight ratio. Eight blastocysts were transferred into uterine horns treated with AM or AM + AM(24–50), and 16 blastocysts were transferred into uterine horns treated with AM + CFH. Recipient females were euthanized 3 days later after a tail vein injection of 0.1 mL 1% Evans blue dye (Sigma-Aldrich) in 0.9% NaCl. Embryo spacing was calculated in ImageJ (NIH) using the quantitation method depicted in Figure 1C.

In vivo barrier permeability assay

Wild-type and *Adm*$^{+/-}$ females at least 8 weeks old were used for timed pregnancies. Visualization of the vaginal plug was considered e0.5. On e7.5, mice were anesthetized with tribromoethanol and injected retro-orbitally with 1 mg biotinylated bovine serum albumin (BSA). Two hours after injection, mice were euthanized, and implantation sites were dissected and fixed overnight in 4% paraformaldehyde at 4°C. Following fixation, implantation sites were cryoprotected in 30% sucrose and frozen in optimal cutting temperature compound for sectioning. Tissue sections were stained with diaminobenzidine to evaluate the extent of BSA penetration toward the embryo.

Wet:dry weight

Day 2.5 pseudopregnant females were treated with a direct intrauterine injection of 0.9% NaCl or 150 pmol AM (4.3 μl) (Phoenix Pharmaceuticals). Thirty minutes later, animals were euthanized and dissected. A segment of uterine tissue was weighed at the time of dissection, incubated in a 60°C oven for 72 h, and then re-weighed.

Optical projection tomography

After fixation in 4% paraformaldehyde, e5.0 implantation sites were transferred to PBS/0.1% Triton X-100 (PBST) and washed overnight at 4°C. Implantation sites were then boiled for 10 min in 10 mM citric acid/0.05% Tween 20 and allowed to cool to room temperature. Tissue was subsequently washed at room temperature for 5 min in PBST, 5 min in ddH_2O, 7 min in ice cold acetone, 5 min in ddH_2O, and 5 min in PBST. The tissue was then blocked overnight at 4°C in 5% normal donkey serum/1% BSA/1% DMSO in PBST. Samples were incubated at 4°C for 1 week in primary antibodies: Cx43 (1:200, Sigma-Aldrich) and FITC-conjugated IB4 lectin (1:100, Sigma-Aldrich) diluted in blocking solution. Samples were washed 7 × 15 min + 1 h in 1% BSA/1% DMSO in PBST and then incubated for 90 min in blocking solution. Secondary antibody (DyLight 594 donkey anti-rabbit, 1:100, Jackson ImmunoResearch) was diluted in blocking solution, and specimens were incubated for 3 days at 4°C. Tissues were then washed 8 × 15 min, transferred to PBST and washed overnight. Briefly, to prepare samples for OPT scanning, implantation sites were embedded in 1% low-melt agarose and dehydrated overnight in methanol at room temperature. Embedded specimens were rendered optically transparent by incubating them in benzyl alcohol and benzyl benzoate for 48 h before being scanned in a BiOPTonics 3001 M Optical Projection Tomography Scanner equipped with Cy2 and Texas Red filter sets.

Scanning electron microscopy

Uterine horns of wild-type CD1 females at least 8 weeks old (Charles River) were injected with 0.9% NaCl; 150 pmol AM; or 150 pmol AM + 3 nmol AM(24–50) on pseudopregnant day 2.5. At the time points specified in Figure 4, the animals were euthanized, and the uteri were dissected and cut open longitudinally. Uteri were submerged in a fixative containing 2% paraformaldehyde/2.5% glutaraldehyde/0.15 M sodium phosphate, pH 7.4, and stored at 4°C overnight to several days before processing. After several washes in buffer, the samples were dehydrated through an ethanol dilution series (30%, 50%, 75%, 90%, 100%, and 100%) and subsequently dried using a Samdri-795 critical point dryer (Tousimis Research Corporation) with liquid carbon dioxide as the transition solvent. The tissue was then mounted onto aluminum scanning electron microscopy stubs with carbon adhesive tabs and was sputter coated with gold:palladium alloy (60:40) to a thickness of 20 nm using a Hummer X Sputter Coater (Anatech, Ltd). Specimens were visualized with a Zeiss Supra 25 field emission scanning electron microscope (Carl Zeiss SMT) using an accelerating voltage of 5 kV. Quantitation of pinopode number, size, and percent area were performed in ImageJ (NIH). Images were batch processed with a macro that binarized, inverted, eroded, and then analyzed each image for particles greater than 0.2 μm in area and with a circularity between 0.3 and 1.00. Alternatively, pinopode number was manually determined using an ImageJ Cell Counter plugin.

Immunofluorescence

Paraffin-embedded tissues were sectioned, deparaffinized, and hydrated. Following antigen retrieval in 10 mM citric acid/0.05% Tween 20, pH 6.0, tissues were permeabilized and then blocked in 5% normal donkey serum. Slides were then incubated overnight at room temperature with primary antibodies: CLDN1 (1:500, Bioworld) or Cx43 (1:200, Sigma-Aldrich). The following day, tissues were washed, blocked, and incubated in the dark for 1–2 h at room temperature in secondary antibodies: donkey anti-rabbit Cy3 (1:200, Jackson ImmunoResearch) or donkey anti-rabbit 594 (1:200, Jackson ImmunoResearch). Stained tissues were imaged on a Nikon E800 fluorescence microscope with an Orca CCD camera (Hamamatsu) and Metamorph software (Molecular Devices).

Cell culture

Ishikawa cells were incubated at 37°C containing 5% CO_2 and cultured in phenol red-free DMEM/F12 (Gibco) + 10% fetal bovine serum (FBS) + 1x penicillin/streptomycin. Transepithelial resistance (TER) of Ishikawa cells was determined using an epithelial volt/ohm meter (World Precision Instruments). The collection of primary human endometrial stromal cells (hESCs) from consenting healthy women was approved by the University of North Carolina at Chapel Hill Institutional Review Board. Human ESCs were incubated at 37°C containing 5% CO_2 and cultured in DMEM/F12 (Gibco) + 10% FBS + 1x penicillin/streptomycin. Human ESCs were artificially decidualized for 5 days in DMEM/F12 + 2% FBS + 1x penicillin/streptomycin + 0.5 mM 8-Br-cAMP (Sigma-Aldrich) + 1 μM medroxyprogesterone 17-acetate (Sigma-Aldrich).

Ussing chamber studies

Confluent Ishikawa cultures in collagen-coated 12 mm Snapwell inserts with 0.4 μm pores (Corning) were pretreated with a vehicle control or 10 nM AM (American Peptide Company/Bachem) before being mounted in Ussing chambers (Physiologic Instruments). Data were collected with the Acquire and Analyze software (Physiologic Instruments). Cultures were bathed in 5 mL of isotonic Krebs-Ringer bicarbonate buffer (37°C) circulated with 95% O_2–5% CO_2 gas on both apical and basolateral sides. Cultures were voltage-clamped, and short circuit current (I_{SC}) and TER were measured at baseline and after addition of 100 μM amiloride apically, 10 μM forskolin apically and basolaterally, 10 μM CFTR inhibitor-172 apically, and 10 μM UTP apically (Sigma-Aldrich).

Water permeability assay

Ishikawa cells were plated on collagen-coated 12 mm transwells with 0.4 μm pores (Corning) and grown to confluency. Water permeability was measured as previously described [24]. Briefly, Ishikawa cells were incubated with 3 μM calcein-AM (Thermo Fisher) for 30 min prior to pretreatment with a vehicle control or 10 nM AM (American Peptide Company/Bachem) for 1 h. Ishikawa cultures were then placed in an Attofluor Cell Chamber with 100 μL of modified Ringer solution added serosally [101 mM NaCl, 12 mM $NaHCO_3$, 24 mM HEPES, 1.2 mM $MgCl_2$, 1.2 mM $CaCl_2 \bullet 2H_2O$, 5.2 mM KCl, 10 mM D-(+)-Glucose (Sigma)]. Isotonic Ringer solution (100 μL) was added apically and a baseline image was obtained. After apical addition of 100 μL of Ringer solution containing an additional 150 mM NaCl (600 mOsm total osmolarity), cultures were imaged on a Leica SP5 confocal microscope over a 30 s period using a 40× water immersion lens (0.9 NA) with calcein excited at 488 nm. Cell height and fluorescence were measured in ImageJ (NIH), and linear regression was performed on the percent change in cell height and fluorescence over time after addition of hypertonic buffer.

Scrape loading assay

Human ESCs were plated in a six-well plate, grown to confluency, and artificially decidualized as described above. Human ESCs were treated with water, 10 nM AM (American Peptide Company/Bachem), 100 μM carbenoxolone (Sigma-Aldrich), or 10 nM AM + 100 μM carbenoxolone for 30 min. Lucifer yellow (Sigma-Aldrich) was added to each well to a final concentration of 0.05%. Decidualized hESC monolayers were then scraped with a 27-G needle, incubated at 37°C for 30 min, and then fixed in 4% paraformaldehyde for 20 min. Cells were then washed and stored in PBS for imaging on an Olympus IX81. Images were analyzed in ImageJ (NIH) by measuring the distance from the scratch to the farthest lucifer yellow dye-positive nucleus in the field. Images were converted to black and white and then inverted in ImageJ for publication. All alterations to brightness and contrast were applied to the entire image.

Statistics

All data are presented as mean ± SEM unless otherwise noted. All statistics were performed in Prism 5 (GraphPad Software, Inc.). Implantation sites per horn following blastocyst transfer were compared by Mann-Whitney test. Unpaired t-tests were used to compare pinopode number, size, and density; uterine wet:dry weight; distance traveled by lucifer yellow dye in the scrape loading assay; and percent penetration to the embryo in the PDZ barrier permeability assay. Embryo spacing was analyzed by unpaired t-test with Welch's correction. The AM treatment time course was analyzed by two-way ANOVA followed by Bonferroni post-tests. If $P < 0.05$, data sets were considered statistically different.

Results

Adrenomedullin treatment improves implantation success and spacing

Given the subfertility of $Adm^{+/-}$ female mice, we first tested whether treating the uterus with AM could support implantation and early pregnancy using an in vitro fertilization (IVF) embryo transfer model. We treated the uterus of wild-type female mice with AM immediately prior to blastocyst transfer and observed a significant increase in the implantation numbers between vehicle- and AM-treated animals at e6.5, an effect that was reversed by co-treatment with the mouse AM inhibitor AM(24–50) (Figure 1A and B). We then attempted to bolster the effect of AM by co-treating with its binding partner, complement factor H (CFH), as has been done by other groups in the context of sepsis [25,26]. However, we found that co-treatment of AM and CFH was antagonistic to implantation and led to fewer

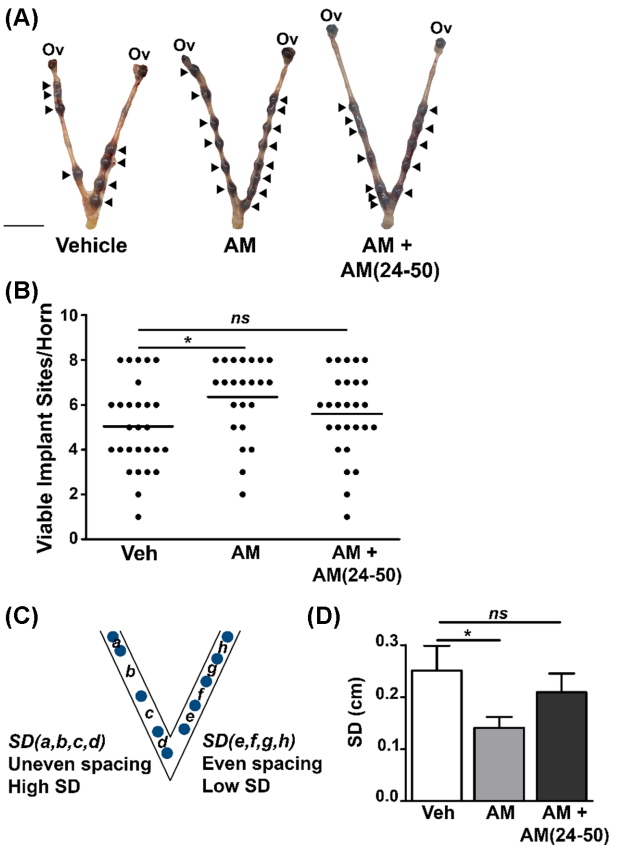

Figure 1. AM improves implantation success and spacing in mice. (A) Images of e6.5 embryos within uteri treated with vehicle, AM, or AM + AM(24–50) prior to transfer of eight blastocysts per horn. Arrowheads indicate viable implantation sites as determined by uptake of Evans blue dye. Scale bar, 1 cm. (B) Quantitation of viable implant sites per horn. Dots represent uterine horns. *ns*, not significant. $^*P < 0.05$, Mann-Whitney test. (C) Illustration of quantitation method for spacing of e6.5 embryos within uterine horns. SD, standard deviation. (D) Quantitation of spacing in vehicle (n = 26), AM (n = 21), and AM + AM(24–50) (n = 25) horns using method depicted in (C). $^*P < 0.05$, unpaired *t* test with Welch's correction.

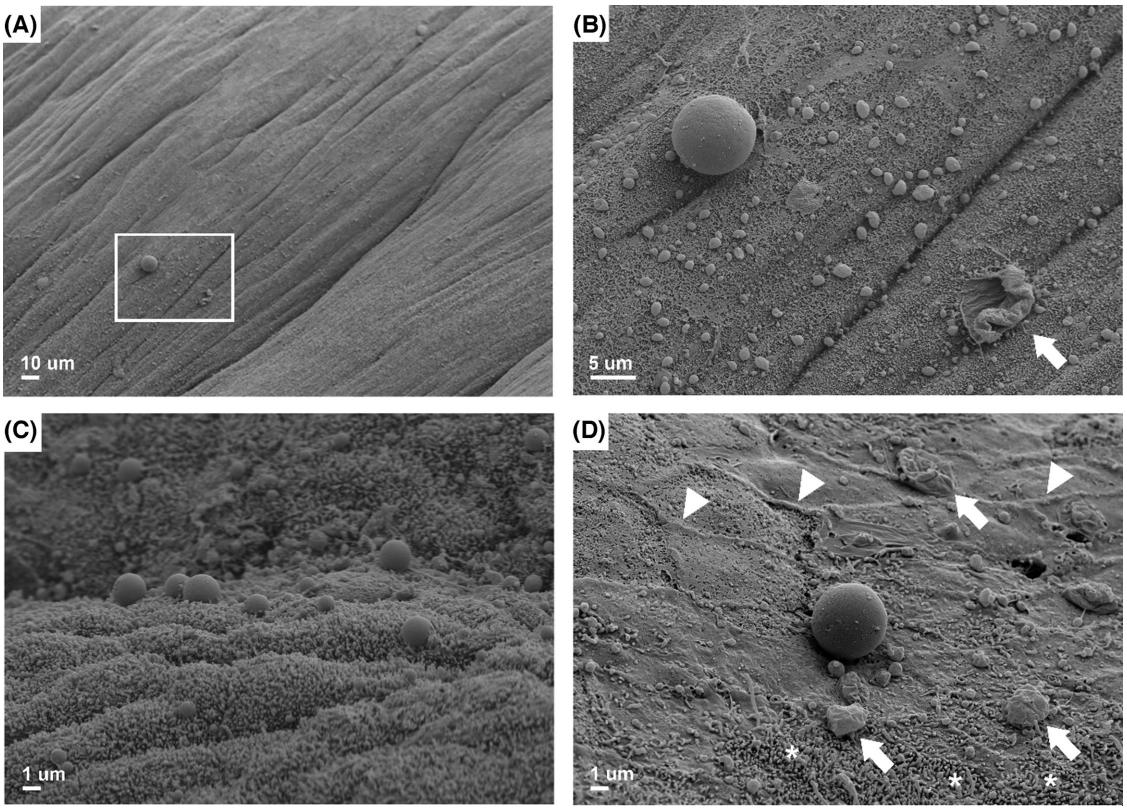

Figure 2. Scanning electron micrographs of pinopodes and other ultrastructural features of uterine epithelial cells in wild-type mice on days 2.5–3.5 of pseudopregnancy. (A) Box encloses the image displayed in (B). Scale bar, 10 μm. (B) Juxtaposition of a single large pinopode and many smaller pinopodes. Arrow points to a potentially degenerate pinopode. Scale bar, 5 μm. (C) Pinopodes projecting above the epithelial cell layer into the lumen of the uterus. Scale bar, 1 μm. (D) Arrows point to potentially degenerate pinopodes. Arrowheads denote examples of cell–cell borders. Asterisks signify area dense in microvilli. Scale bar, 1 μm.

viable implantation sites at e6.5 compared to vehicle-treated animals (data not shown).

Our previously published embryonic spacing defect in the $Adm^{+/-}$ subfertile female mice then prompted us to compare the spacing patterns of embryos of vehicle- and AM-treated animals [12]. To quantify embryonic spacing, we calculated the standard deviation of distances between the implant sites within each uterine horn (Figure 1C). Using this method, we found that the standard deviation was significantly lower in AM-treated uterine horns, indicating that these embryos were more evenly spaced relative to each other compared to their vehicle-treated counterparts (Figure 1D).

Adrenomedullin promotes epithelial pinopode formation

We then analyzed the luminal epithelium of vehicle- and AM-treated uteri for the presence of pinopodes: spherical protrusions of the epithelial plasma membrane into the lumen of the uterus that are present in mice and humans during the window of implantation and associated with uterine receptivity [27]. We previously discovered that the epithelial surfaces of $Adm^{+/-}$ uteri present fewer pinopodes, underscoring our rationale for investigating AM-mediated effects on pinopode dynamics [12]. Scanning electron microscopy enabled visualization of pinopodes as large as 10 μm in diameter even at low magnification (Figure 2A). At higher power, many smaller pinopodes of approximately 1 μm in diameter were visible in areas surrounding larger pinopodes (Figure 2B). Interestingly, we observed three-dimensional structures that were similarly sized as pinopodes but appeared collapsed or degenerate, raising the compelling possibility that these structures are pinopodes captured in various stages of formation or regression (Figure 2B, arrow). On the horizon of a plane orthogonal to the uterine luminal epithelial landscape, we captured the topography of pinopodes protruding prominently above the epithelial surface (Figure 2C). Upon closer inspection of a single, large pinopode, we again noted several smaller pinopodes in its shadow as well as larger degenerate pinopodes in the surrounding area (Figure 2D, arrows). We were also able to visualize other ultrastructural features of the epithelium, such as cell–cell borders and small, rod-like microvilli (Figure 2D, arrowheads and asterisks).

We then analyzed the direct effect of AM on pinopode formation by performing a time course study, treating wild-type pseudopregnant uteri for 30 min, 2 h, 6 h, or 24 h. A 30 min treatment of the uterus with AM significantly enhanced pinopode number as well as pinopode size (Figure 3A–C). Ultimately, a significantly larger percentage of the epithelial surface was covered by pinopodes in AM-treated uteri compared to vehicle-treated uteri (Figure 3D). We observed a complete reversal of these AM-mediated changes by co-treating with AM and its inhibitor, AM(24–50) (Figure 3A–D).

Quantitation of pinopode density beyond the 30 min time point revealed a common pinopode formation and regression pattern between days 2.5 and 3.5 of pseudopregnancy: first, an enhancement of pinopode number between 2 and 6 h, followed by a decline between 6 and 24 h, and an eventual return to levels comparable to those at 30 min (Figure 4A). However, in the AM-treated uteri, we observed

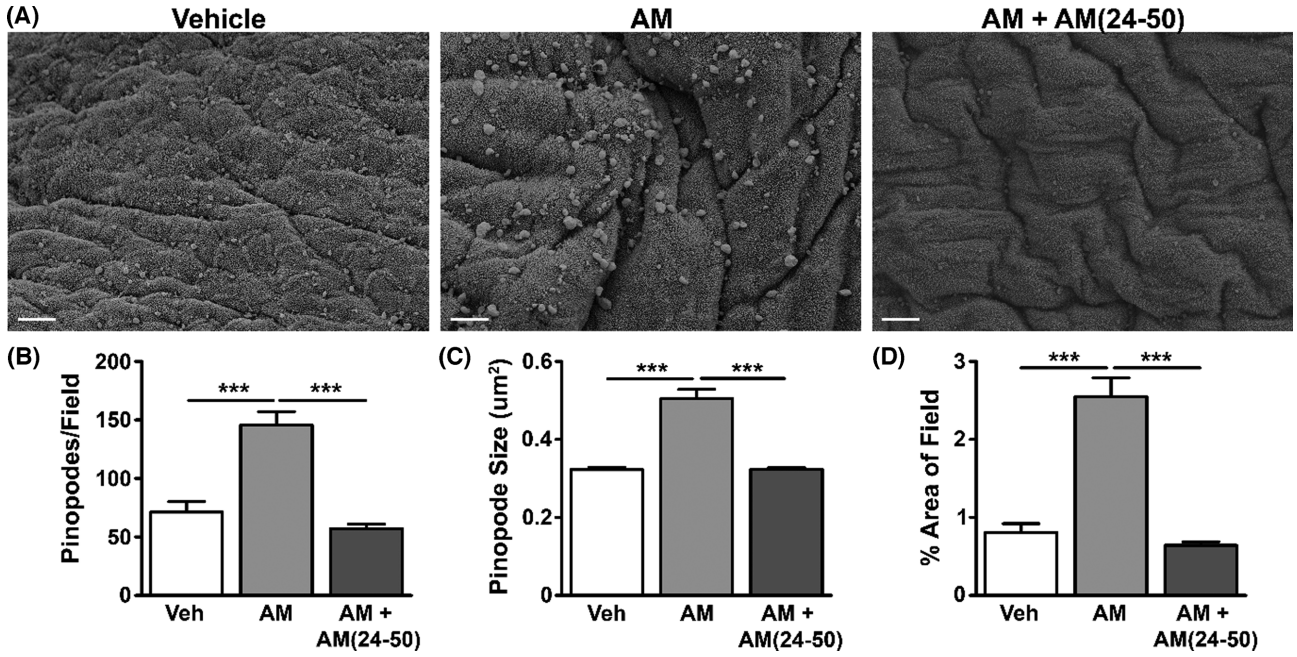

Figure 3. AM promotes pinopode formation and size. (A) Scanning electron micrographs of pinopodes in wild-type pseudopregnant uteri treated with vehicle, AM, or AM + AM (24–50) for 30 min. Scale bars, 5 μm. (B–D) Quantitation of pinopodes per field (B), size (C), and percent area of field (D). n $\geq$ four fields from n $\geq$ three animals per treatment group. $^{***}P < 0.001$, unpaired *t* test.

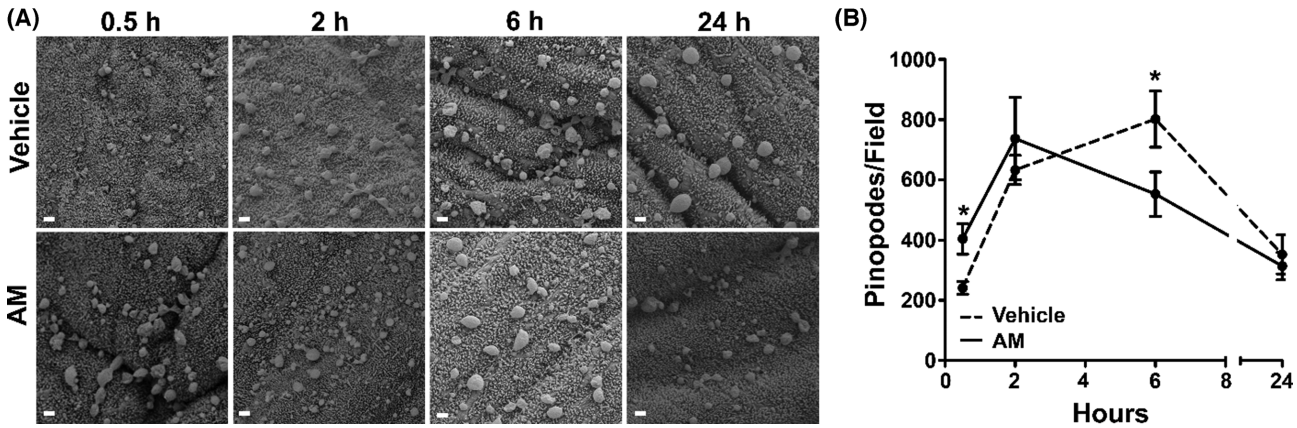

Figure 4. AM accelerates pinopode formation dynamics in wild-type mice between days 2.5 and 3.5 of pseudopregnancy. (A) Scanning electron micrographs of vehicle- and AM-treated uteri throughout treatment time course. Scale bars, 1 μm. (B) Quantitation of pinopodes per field throughout treatment time course. n $\geq$ six fields total from n = three animals per treatment group. $^{*}P < 0.05$ at indicated time point, Bonferroni post-tests following two-way ANOVA.

an early leftward shift of this curve, demonstrating the ability of AM to acutely stimulate pinopode dynamics during early pregnancy (Figure 4B). There was a statistically significant interaction between the effects of time and treatment on pinopode number by two-way ANOVA ($P = 0.003$), and Bonferroni post-tests identified significant differences in pinopode number after 30 min and 6 h of treatment.

Adrenomedullin accelerates uterine water transport across the epithelium

While little is understood about the dynamics of pinopode formation and function, several groups have proposed that pinopodes pinocytose uterine fluid [28,29]. Therefore, to determine whether AM-mediated pinopode formation was associated with enhanced uterine water transport in vivo, we treated wild-type pseudopregnant uteri with AM and measured uterine wet:dry weight. We compared vehicle- and AM-treated uteri and, consistent with our hypothesis, found that the wet:dry weight ratio was significantly higher in AM-treated uteri (Figure 5A).

We then asked whether AM enhanced the uterine wet:dry weight ratio by altering epithelial ion transport or epithelial water permeability and subsequent water transport using Ishikawa cells, which are derived from an endometrial adenocarcinoma and display a hybrid phenotype between uterine glandular and luminal epithelium [30,31]. Ishikawa cells form confluent monolayers and express an array of epithelial-specific proteins, including keratins [32], integrins [33], and tight junctions such as claudin 1 (*Cldn1*, CLDN1) (data not shown). Furthermore, Ishikawa cells are moderately polarized [34] and generate an average TER of approximately 350 Ω after 4 days in culture (Figure 5B).

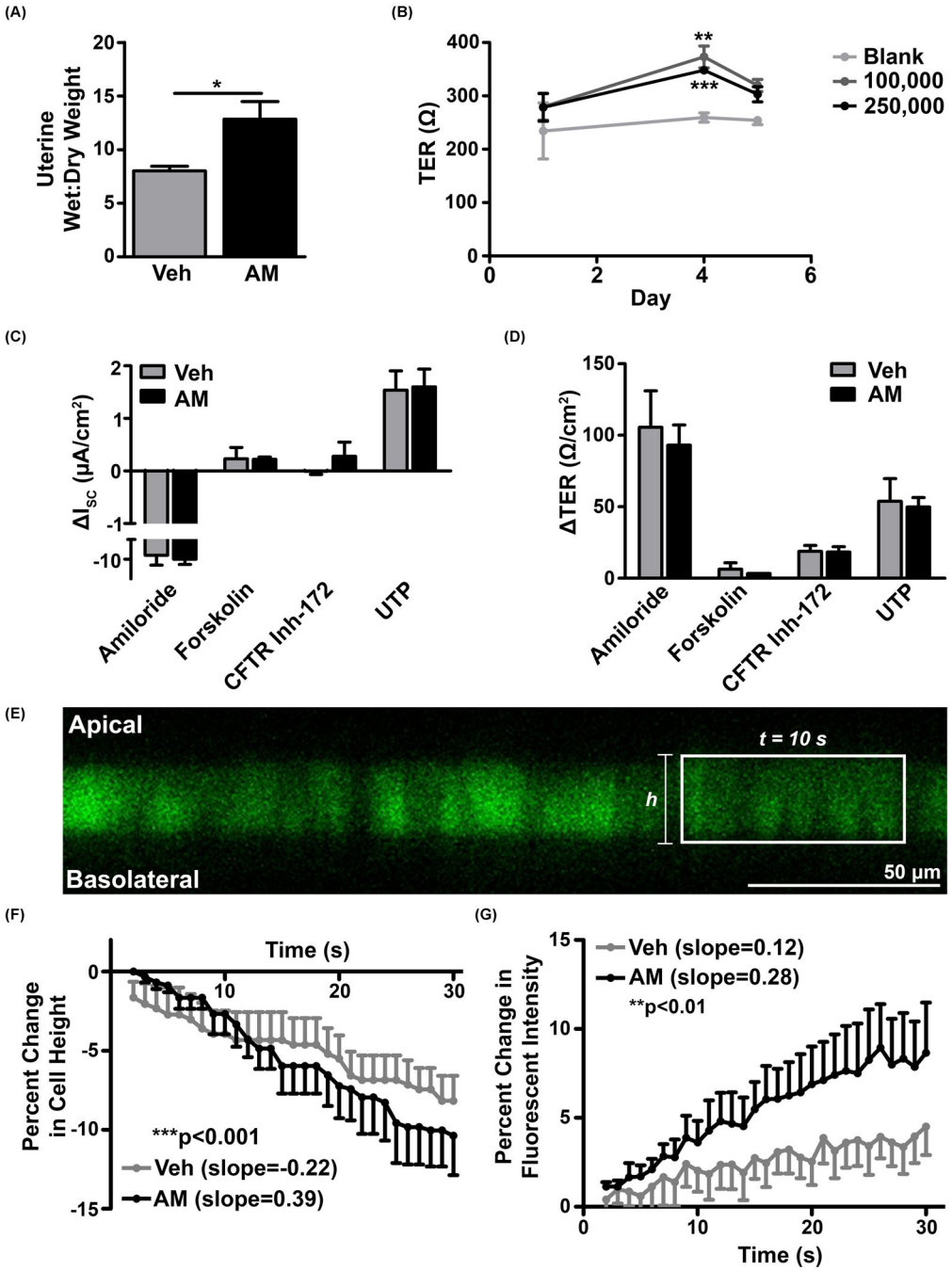

Figure 5. AM enhances uterine wet:dry weight in vivo and water transport across Ishikawa cells in vitro. (A) Wet:dry weight ratio of wild-type uteri on day 2.5 of pseudopregnancy. n = three animals per treatment group. $^{*}P < 0.05$, unpaired *t* test. (B) Change in transepithelial resistance (TER) of Ishikawa cells seeded at densities of 100,000 and 250,000 cells per transwell compared to a blank transwell between days 1 and 5 of culture. n ≥ three cultures per time point. $^{**}P < 0.01$, $^{***}P < 0.001$, unpaired *t* test at each density compared to blank. (C and D) Changes in short-circuit current (C) and TER (D) after addition of activators and inhibitors of ion channels following vehicle- and AM-pre-treated cultures (n = three per pre-treatment group). (E) Representative image of calcein-loaded Ishikawa cells used in water permeability experiment. Rectangle encloses representative series of adjacent cells analyzed for changes in cell height and fluorescence after addition of hypertonic solution. Scale bar, 50 μm. (F) Percent change in Ishikawa cell height after vehicle (n = five cumulative treatments from three cultures) and AM (n = six cumulative treatments from three cultures) pretreatment followed by hypertonic shock. Data are presented as mean + SEM (vehicle) or mean – SEM (AM). Slopes were calculated by linear regression analysis. $^{***}P < 0.001$, ANCOVA. (G) Percent change in calcein fluorescent intensity after hypertonic shock. Data are presented as mean – SEM (vehicle) or mean + SEM (AM). Slopes were calculated by linear regression analysis. $^{**}P < 0.01$, ANCOVA.

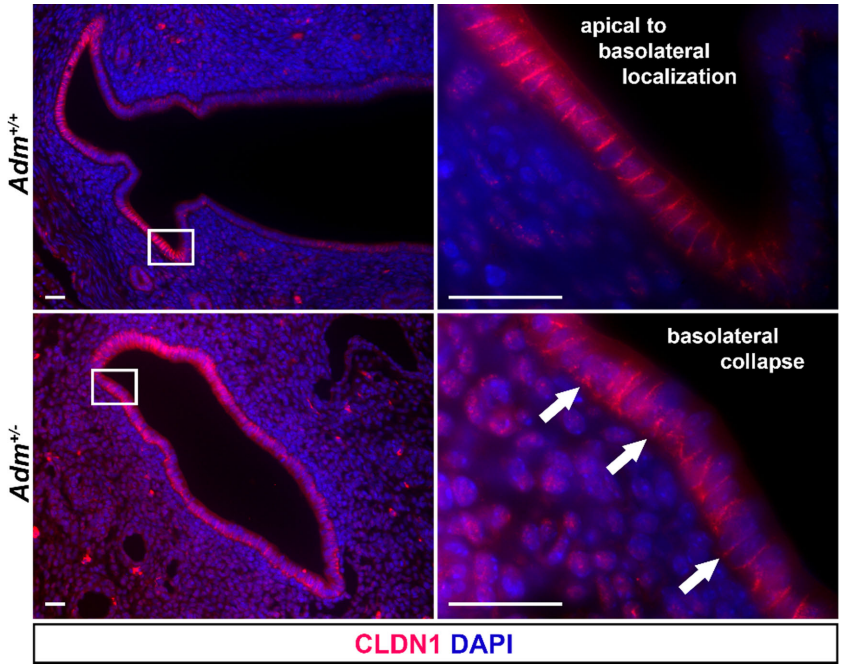

Figure 6. AM contributes to proper CLDN1 localization. Immunohistochemistry for CLDN1 in wild-type (n = 3) and $Adm^{+/-}$ (n = 4) e5.5 interimplantation sites. Arrows denote CLDN1 localization, spanning the apical-basolateral axis of epithelial cell lateral borders ($Adm^{+/+}$) or concentrated on the basolateral side of the epithelial cell layer ($Adm^{+/-}$). Scale bars, 20 μm.

We first performed Ussing chamber studies in Ishikawa cells to assess effects on ion transport by measuring changes in epithelial short-circuit current (I_{SC}) and TER in response to AM and the following channel modulators: amiloride, an epithelial sodium channel (ENaC) inhibitor; forskolin, which induces cAMP activation of the cystic fibrosis transmembrane conductance regulator (CFTR); CFTR inhibitor-172; and UTP, an activator of calcium-activated chloride channels. Pretreatment of Ishikawa cells with AM did not affect changes in I_{SC} and TER in response to this series of ion channel activators and inhibitors, indicating that AM does not affect uterine water balance by altering ion transport (Figure 5C and D). Notably, modulation of CFTR activity conferred negligible changes in I_{SC} and TER, which is consistent with low expression of *CFTR* in Ishikawa cells (data not shown).

We then assessed whether AM affects water permeability of the Ishikawa cell apical membrane by confocal microscopy. Following the addition of a hypertonic buffer solution on the apical Ishikawa membrane to create an osmotic gradient, we observed a significant enhancement in the rate of both Ishikawa cell shrinkage and calcein fluorescent intensification with AM pretreatment compared to vehicle pretreatment, indicating that AM enhances the rate of water transport across the apical surface of Ishikawa cells (Figure 5F and G). Altogether, these data support a role for AM in primary water transport, but not ion transport, in the uterus.

AM ensures appropriate epithelial CLDN1 localization

The junctional protein CLDN1 plays essential roles in water homeostasis in epithelial barriers. For example, genetic deletion of *Cldn1* in mice confers lethality by postnatal day 1 due to defective epidermal barrier formation and consequent water loss [35]. Previously published associations between epithelial cell junction integrity and fertility prompted us to examine the localization of CLDN1 [16,18]. Therefore, we employed our murine model of *Adm* haploinsufficiency and subfertility to investigate the effect of AM on CLDN1 localization in the pregnant uterine epithelium. In wild-type pregnant uteri, we observed continuous CLDN1 expression from the apical to the basolateral sides of the epithelium along the lateral borders of cells. However, in $Adm^{+/-}$ pregnant uteri, we noted collapse of CLDN1 to the basolateral side of the luminal epithelium (Figure 6). In all animals of both genotypes, we observed circumferentially patchy expression of CLDN1 around the lumen. These data indicate that even a modest change in the local production of AM in the uterus can influence the localization of epithelial barrier proteins during the peri-implantation period.

AM enhances stromal gap junction communication and barrier integrity

We next turned our attention to uterine stroma, which includes the PDZ adjacent to the embryo as an additional site of robust *Adm* and cell junction expression during the peri-implantation period [11]. Decidualized stromal cells communicate with each other to organize this complex, three-dimensional structure, which provides an early protective barrier to promote successful implantation. Accordingly, we confirmed that the gap junction protein Cx43, which facilitates intercellular communication, is highly expressed in the early implantation site using three-dimensional optical projection tomography (Figure 7A and B). To assess the direct effect of AM on Cx43 in uterine stroma, we treated pseudopregnant uteri with AM and performed immunohistochemistry for Cx43, finding that AM treatment enhanced Cx43 expression in stroma adjacent to the luminal epithelium—the future site of the PDZ (Figure 7C).

We then functionally evaluated whether AM could influence gap junction coupling between stromal cells by using primary hESCs to perform a scrape loading assay. In this assay, cells are "scratched"

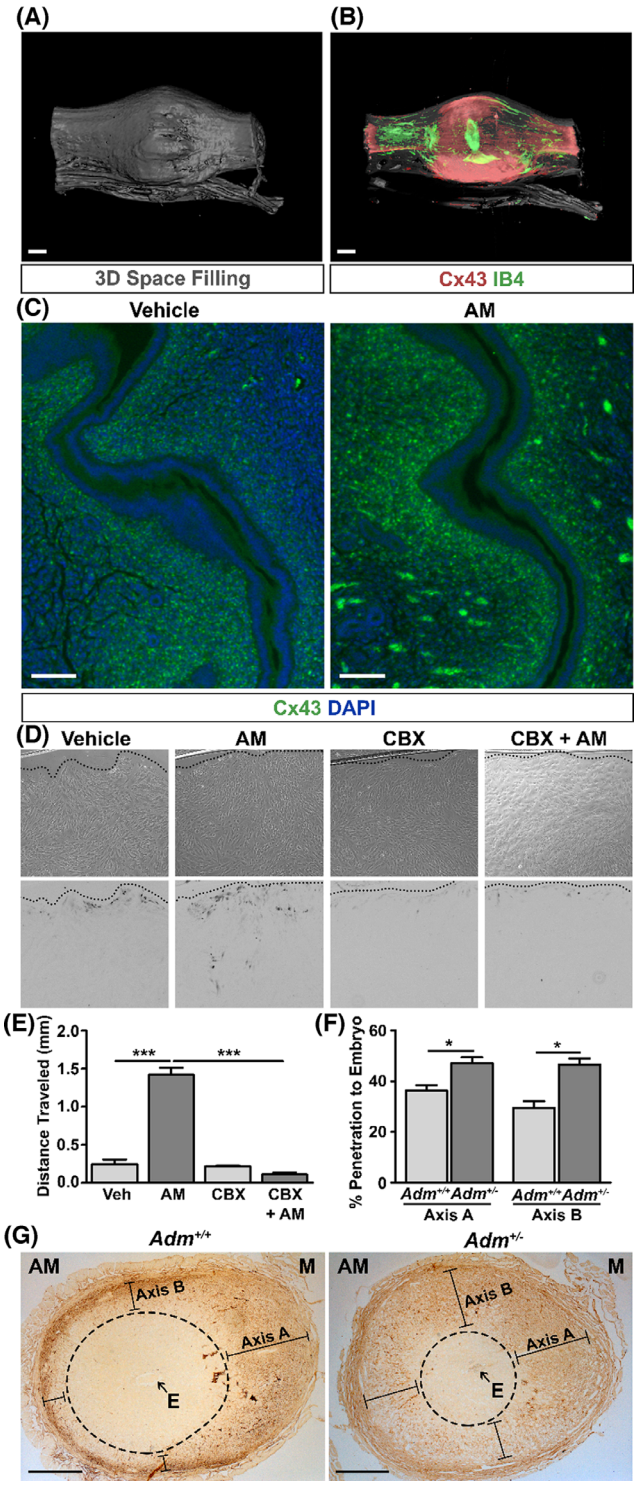

Figure 7. AM enhances gap junction expression and communication in uterine stroma. (A and B) Optical projection tomography (OPT) three-dimensional space filling scan (A) and Cx43 expression scan (B) of a wild-type e5.0 implantation site and adjacent interimplantation sites. IB4 lectin staining indicates endothelium and embryonic tissue. Scale bars, 400 μm. (C) Immunohistochemistry for Cx43 in pseudopregnant uteri treated with vehicle or AM for 30 min. Clusters of signal at the periphery of the AM image are autoflurescent red blood cells. n = three animals per treatment group. Scale bars, 100 μm. (D) Bright field (top) and inverted fluorescent (bottom) images of a scrape loading assay in hESCs. Dotted lines indicate location of the scrape. (E) Quantitation of distance traveled by lucifer yellow dye from the scrape. CBX, carbenoxolone, a gap junction inhibitor. n = three fields per treatment group. $^{***}P < 0.001$, unpaired *t* test. (F) Quantitation of distance traveled by biotinylated BSA toward the embryo of e7.5 $Adm^{+/+}$ (n $\geq$ 7 per axis) and $Adm^{+/-}$ (n $\geq$ 25 per axis) implantation sites as a percentage of the total length of the axes depicted in (G). $^{*}P < 0.05$, unpaired *t* test. (G) Representative images of e7.5 $Adm^{+/+}$ and $Adm^{+/-}$ implantation sites stained for diaminobenzidine to assess the penetration of biotinylated BSA toward the embryo. The area within the dashed ellipses represents the zone not penetrated by BSA. Lines represent distance traveled by BSA toward embryo and quantitated in (F). Scale bars, 0.5 mm. AM, anti-mesometrial side; E, embryo; M, mesometrial side.

open, and the distance of transfer of a gap junction-permeable dye, lucifer yellow, is measured across the monolayer. Interestingly, AM promoted functional gap junction coupling between hESCs as evidenced by the enhanced distance of lucifer yellow dye transfer across the cell monolayer. This effect was abrogated by co-treatment with the gap junction inhibitor carbenoxolone (Figure 7D and E).

We hypothesize that communication between stromal cells via gap junctions provides cues that direct the formation of the PDZ, which forms a selective barrier around the embryo. Therefore, given the effect of AM on cellular communication, we assessed the consequences of a reduction in AM peptide on the selectivity of this barrier in vivo. We examined the integrity of the PDZ in wild-type and $Adm^{+/-}$ female mice by injecting pregnant mice retro-orbitally with biotinylated BSA and then assessing the depth of BSA penetration into the decidua toward the embryo on two different axes of the implantation site. In $Adm^{+/-}$ females, BSA penetrated significantly closer to the embryo compared to wild-type animals, indicating compromised PDZ barrier function in heterozygous decidua (Figure 7F and G). Altogether, these data serve as evidence for a role for AM in stromal cell communication and PDZ barrier formation in support of early pregnancy and point to additional mechanistic insight into how AM promotes pregnancy success.

Discussion

Here, we have elucidated molecular and cellular effects of AM on the epithelial and stromal compartments of the uterus during the peri-implantation period. Moreover, we demonstrate that administration of AM directly into the uterus enhances the embryo implantation rate in mice after blastocyst transfer, suggesting a potential use for AM peptide in the context of embryo transfer or IVF in humans.

There is intense interest in improving the IVF live birth rate, which currently stands at less than 50%. Advances in clinical embryology have enabled the identification of aneuploid embryos prior to transfer, but the IVF live birth rate remains low because we do not completely understand uterine factors supporting implantation. Despite this lack of understanding, attempts have been made to overcome endometrial receptivity defects. For example, systemic G-CSF treatment has been shown in a single randomized controlled trial to benefit women with recurrent implantation failure but not provide benefit to other women [36]. Endometrial scratching, in which the endometrium is physically injured to provoke an inflammatory response, is currently being recommended by practitioners in some countries to many women refractory to IVF [37]. However, the mechanisms of action following this invasive procedure remain unclear. Furthermore, inflammation, if uncontrolled, may be associated with abnormal implantation and pregnancy complications [38]. Therefore, direct, short-term treatment of the endometrium with AM peptide may provide an attractive and more efficacious

alternative to either a systemically administered drug or an inflammation-provoking injury.

Unexpectedly, we found that co-administration of AM and CFH, which binds and stabilizes AM in plasma, was antagonistic to embryo implantation [39]. In addition to associating with AM, CFH blocks activation of the alternative complement pathway, deterring aberrant complement deposition by facilitating the distinction between self and nonself cells [40]. Unfortunately, very little is known about the role of complement in embryo implantation and the establishment of pregnancy. Recently, two groups found that activation of complement is associated with embryo loss in both mice and humans [41,42]. As we begin to appreciate the proinflammatory environment of embryo implantation, we believe it is possible that exogenous administration of high levels of CFH caused dysregulation of fine-tuned, physiological complement and inflammatory responses that are critical for implantation success [43].

Notably, in our study, AM improved not only the implantation rate but also the spacing between embryos in utero. How embryos space within the mouse uterine horn is not completely understood and, at first glance, appears irrelevant for singleton human pregnancies [44]. However, what we learn about embryo spacing can certainly inform our understanding of embryo–uterine interactions and the choice of implantation location, which are highly relevant for both singleton and multifetal gestations, especially given the programming of clinical complications of pregnancy by implantation defects [2].

Subsequently, we found that AM treatment of the uterus promotes pinopode formation, size, and epithelial surface coverage. Only a handful of descriptive studies provide information on pinopodes, with the average mouse pinopode quantified at approximately 6 μm in diameter [45]. Indeed, we identified pinopodes at least 6 μm in diameter, but the majority of pinopodes we observed were approximately 1 μm in diameter. These differences in size could be explained by differences in genetic backgrounds, by visualization of the uterus at different time points during pregnancy, or by different effects of pseudopregnancy. We frequently observed what appeared to be ruptured pinopodes in various stages of growth or regression. Ruptured pinopodes have been observed in both rodents and humans, but more frequently in the latter species [46,47]. Other groups have argued that pinopode coverage of the epithelium ranges from 0.6% to 20% [45]; our studies were consistent with these findings.

Pinopodes may pinocytose uterine fluid, ultimately affecting uterine water balance in support of implantation, though this hypothesis has been largely supported in rats and less so in humans [28,29,48,49]. We found that AM accelerated water loss across the apical Ishikawa cell membrane in the context of hypertonic stress, suggesting that AM renders the apical Ishikawa cell membrane more permeable to water. Early in the peri-implantation period, uterine water imbibition causes an estrogen-induced accumulation of water in the uterine lumen via the transcellular pathway, ultimately changing luminal fluid viscosity to facilitate an environment amenable to implantation; this occurs in part by altering aquaporin expression and availability [50–52]. In the mouse, expression of aquaporins-2, -3, and -4 has been observed in uterine luminal epithelium, suggesting that these aquaporins may participate in the accumulation of water in the uterine lumen [51,52]. However, at the time of implantation, water transport also occurs in the opposite direction at the time of closure of the uterine epithelium around an implanting blastocyst [53]. Therefore, water transport across the uterine luminal epithelium occurs bidirectionally during the peri-implantation period.

Our findings of enhanced uterine wet:dry weight and accelerated water transport across Ishikawa cells with AM treatment show that AM may contribute to this water transport to promote implantation. In further support of this idea, estrogen is a potent regulator of uterine water transport, aquaporins, and *Adm* gene expression—both directly through estrogen response elements in the 5′ untranslated region and indirectly through an estrogen-induced cohort of miRNAs targeting the 3′ untranslated region of the *Adm* gene [54,55]. Given the uterine wet:dry weight data, it is likely that AM stimulates water transport from the uterine lumen to the uterine wall, possibly through pinopodes, although the tissue compartments in which this water accumulates have yet to be determined. The uterine wet:dry weight may also be explained in part by effects of AM on circulatory and lymphatic vascular systems, but the direct vascular effects on the uterus in our AM-supplemented blastocyst transfer model are currently unknown.

Given the lethal water loss phenotype of mouse embryos lacking the tight junction protein CLDN1, we utilized our subfertile $Adm^{+/-}$ mice to investigate the effect of AM on CLDN1 localization in the uterine epithelium. Analysis of subfertile $Adm^{+/-}$ uterine epithelium suggested a role for AM in appropriate localization of CLDN1. Notably, this is not the first association between aberrant cell junctional protein expression and localization and uterine receptivity defects. Both an epithelial-specific deletion of *Stat3* and a panuterine deletion of *Msx1/Msx2* on day 4 of pregnancy or pseudopregnancy, respectively, demonstrate anomalous CLDN1 expression and infertility [16,18]. More specifically, in each of these transcription factor loss-of-function studies, CLDN1 was persistently expressed in epithelium, while it was absent in floxed control animals. Therefore, Pawar and colleagues concluded that the repression of *Cldn1* facilitates a requisite loss of cell polarity during early implantation [16]. Our observations of aberrant CLDN1 localization in epithelium heterozygous for *Adm* support a role for AM in epithelial cell organization, which has consequences for uterine receptivity and epithelial remodeling during implantation.

In this study, we also investigated the effects of AM on uterine stroma during peri-implantation, concluding that AM promotes Cx43 expression in the uterus, stromal intercellular communication, and organization of the PDZ. Our conclusion concerning the effect of AM on Cx43 expression is consistent with our previously published study in lymphatic endothelium [22]. The importance of Cx43 and gap junction-mediated intercellular communication in the uterus is highlighted by the effects of conditional knockout of Cx43 in the uterus, which negatively affects decidualization, expression of angiogenic factors, and placental angiogenesis, ultimately leading to fetal loss [56]. Furthermore, *Adm* gene expression is upregulated twofold in stroma from $Msx1^{d/d}/Msx2^{d/d}$ uteri, possibly in a compensatory fashion to support the implantation defects in these animals [18].

Together, the effects of AM on pinopodes, water permeability, and cell junctions in the epithelial and stromal compartments of the uterus during peri-implantation synergize to support implantation, as evidenced by our finding that treatment of the mouse uterus with AM prior to blast transfer improves the implantation rate. This discovery complements elegant studies performed by Yallampalli and colleagues in rats, finding that continuous administration of the human AM inhibitor, AM(22–52), via osmotic minipumps is detrimental to implantation and placentation [57,58]. Similarly, genetic loss of *Adm* expression in the fetal placenta causes under-recruitment of uterine natural killer cells and a loss of spiral artery remodeling,

phenotypes consistent with the development of preeclampsia, a dangerous placenta-driven complication of pregnancy [59]. Consistent with murine data, we previously found the biomarker mid-regional pro-adrenomedullin (MR-proADM) to be reduced in women with severe preeclampsia and a polymorphism within the human *Adm* gene to be associated with reduced birth weight, highlighting its relevance to human pregnancy [60,61]. In summary, our findings provide molecular insights into the compartmental effects of AM signaling in the uterus during peri-implantation and highlight a potential therapeutic for poor implantation, possibly in the context of ART. Most importantly, studies addressing the safety and efficacy of intrauterine delivery of AM in humans are merited and may have the potential to improve fertility rates.

Acknowledgments

The authors acknowledge the Animal Models Core; the Animal Histopathology Core; the Histology Research Core Facility; and the Microscopy Services Laboratory, all at the University of North Carolina at Chapel Hill, for their assistance.

References

1. Wang H, Dey SK. Roadmap to embryo implantation: clues from mouse models. *Nat Rev Genet* 2006; **7**:185–199.
2. Cha J, Sun X, Dey SK. Mechanisms of implantation: strategies for successful pregnancy. *Nat Med* 2012; **18**:1754–1767.
3. Cha J, Dey SK. Cadence of procreation: orchestrating embryo-uterine interactions. *Semin Cell Dev Biol* 2014; **34**:56–64.
4. Hantak AM, Bagchi IC, Bagchi MK. Role of uterine stromal-epithelial crosstalk in embryo implantation. *Int J Dev Biol* 2014; **58**: 139–146.
5. Scott RT, Jr, Ferry K, Su J, Tao X, Scott K, Treff NR. Comprehensive chromosome screening is highly predictive of the reproductive potential of human embryos: a prospective, blinded, nonselection study. *Fertil Steril* 2012; **97**:870–875.
6. Li Y, Sun X, Dey SK. Entosis allows timely elimination of the luminal epithelial barrier for embryo implantation. *Cell Rep* 2015; **11**:358–365.
7. Ramathal CY, Bagchi IC, Taylor RN, Bagchi MK. Endometrial decidualization: of mice and men. *Semin Reprod Med* 2010; **28**:17–26.
8. Rogers PA, Murphy CR, Rogers AW, Gannon BJ. Capillary patency and permeability in the endometrium surrounding the implanting rat blastocyst. *Int J Microcirc Clin Exp* 1983; **2**:241–249.
9. Lenhart PM, Caron KM. Adrenomedullin and pregnancy: perspectives from animal models to humans. *Trends Endocrinol Metab* 2012; **23**:524–532.
10. Matson BC, Caron KM. Adrenomedullin and endocrine control of immune cells during pregnancy. *Cell Mol Immunol* 2014; **11**:456–459.
11. Li M, Wu Y, Caron KM. Haploinsufficiency for adrenomedullin reduces pinopodes and diminishes uterine receptivity in mice. *Biol Reprod* 2008; **79**:1169–1175.
12. Li M, Yee D, Magnuson TR, Smithies O, Caron KM. Reduced maternal expression of adrenomedullin disrupts fertility, placentation, and fetal growth in mice. *J Clin Invest* 2006; **116**:2653–2662.
13. Luan L, Ding T, Stinnett A, Reese J, Paria BC. Adherens junction proteins in the hamster uterus: their contributions to the success of implantation. *Biol Reprod* 2011; **85**:996–1004.
14. Paria BC, Zhao X, Das SK, Dey SK, Yoshinaga K. Zonula occludens-1 and E-cadherin are coordinately expressed in the mouse uterus with the initiation of implantation and decidualization. *Dev Biol* 1999; **208**:488–501.
15. Wang X, Matsumoto H, Zhao X, Das SK, Paria BC. Embryonic signals direct the formation of tight junctional permeability barrier in the decidualizing stroma during embryo implantation. *J Cell Sci* 2004; **117**:53–62.
16. Pawar S, Starosvetsky E, Orvis GD, Behringer RR, Bagchi IC, Bagchi MK. STAT3 regulates uterine epithelial remodeling and epithelial-stromal crosstalk during implantation. *Mol Endocrinol* 2013; **27**: 1996–2012.
17. Daikoku T, Cha J, Sun X, Tranguch S, Xie H, Fujita T, Hirota Y, Lydon J, DeMayo F, Maxson R, Dey SK. Conditional deletion of Msx homeobox genes in the uterus inhibits blastocyst implantation by altering uterine receptivity. *Dev Cell* 2011; **21**:1014–1025.
18. Sun X, Park CB, Deng W, Potter SS, Dey SK. Uterine inactivation of muscle segment homeobox (Msx) genes alters epithelial cell junction proteins during embryo implantation. *FASEB J* 2016; **30**:1425–1435.
19. Diao H, Xiao S, Howerth EW, Zhao F, Li R, Ard MB, Ye X. Broad gap junction blocker carbenoxolone disrupts uterine preparation for embryo implantation in mice. *Biol Reprod* 2013; **89**:31.
20. Winterhager E, Gellhaus A, Blois SM, Hill LA, Barr KJ, Kidder GM. Decidual angiogenesis and placental orientation are altered in mice heterozygous for a dominant loss-of-function Gja1 (connexin43) mutation. *Biol Reprod* 2013; **89**:111.
21. Dunworth WP, Fritz-Six KL, Caron KM. Adrenomedullin stabilizes the lymphatic endothelial barrier in vitro and in vivo. *Peptides* 2008; **29**:2243–2249.
22. Karpinich NO, Caron KM. Gap junction coupling is required for tumor cell migration through lymphatic endothelium. *Arterioscler Thromb Vasc Biol* 2015; **35**:1147–1155.
23. Caron KM, Smithies O. Extreme hydrops fetalis and cardiovascular abnormalities in mice lacking a functional Adrenomedullin gene. *Proc Natl Acad Sci U S A* 2001; **98**:615–619.
24. Astrand AB, Hemmerling M, Root J, Wingren C, Pesic J, Johansson E, Garland AL, Ghosh A, Tarran R. Linking increased airway hydration, ciliary beating, and mucociliary clearance through ENaC inhibition. *Am J Physiol Lung Cell Mol Physiol* 2015; **308**:L22–L32.
25. Yang S, Zhou M, Chaudry IH, Wang P. Novel approach to prevent the transition from the hyperdynamic phase to the hypodynamic phase of sepsis: role of adrenomedullin and adrenomedullin binding protein-1. *Ann Surg* 2002; **236**:625–633.
26. Yang S, Zhou M, Fowler DE, Wang P. Mechanisms of the beneficial effect of adrenomedullin and adrenomedullin-binding protein-1 in sepsis: down-regulation of proinflammatory cytokines. *Crit Care Med* 2002; **30**:2729–2735.
27. Quinn CE, Casper RF. Pinopodes: a questionable role in endometrial receptivity. *Hum Reprod Update* 2009; **15**:229–236.
28. Enders AC, Nelson DM. Pinocytotic activity of the uterus of the rat. *Am J Anat* 1973; **138**:277–299.
29. Parr MB, Parr EL. Uterine luminal epithelium: protrusions mediate endocytosis, not apocrine secretion, in the rat. *Biol Reprod* 1974; **11**:220–233.
30. Hannan NJ, Paiva P, Dimitriadis E, Salamonsen LA. Models for study of human embryo implantation: choice of cell lines? *Biol Reprod* 2010; **82**:235–245.
31. Nishida M, Kasahara K, Kaneko M, Iwasaki H, Hayashi K. Establishment of a new human endometrial adenocarcinoma cell line, Ishikawa cells, containing estrogen and progesterone receptors. *Nihon Sanka Fujinka Gakkai Zasshi* 1985; **37**:1103–1111.
32. Mo B, Vendrov AE, Palomino WA, DuPont BR, Apparao KB, Lessey BA. ECC-1 cells: a well-differentiated steroid-responsive endometrial cell line with characteristics of luminal epithelium. *Biol Reprod* 2006; **75**:387–394.
33. Castelbaum AJ, Ying L, Somkuti SG, Sun J, Ilesanmi AO, Lessey BA. Characterization of integrin expression in a well differentiated endometrial adenocarcinoma cell line (Ishikawa). *J Clin Endocrinol Metab* 1997; **82**:136–142.
34. Heneweer C, Schmidt M, Denker HW, Thie M. Molecular mechanisms in uterine epithelium during trophoblast binding: the role of small GTPase RhoA in human uterine Ishikawa cells. *J Exp Clin Assist Reprod* 2005; **2**:4.
35. Furuse M, Hata M, Furuse K, Yoshida Y, Haratake A, Sugitani Y, Noda T, Kubo A, Tsukita S. Claudin-based tight junctions are crucial for the mammalian epidermal barrier: a lesson from claudin-1-deficient mice. *J Cell Biol* 2002; **156**:1099–1111.

36. Aleyasin A, Abediasl Z, Nazari A, Sheikh M. Granulocyte colony-stimulating factor in repeated IVF failure, a randomized trial. *Reproduction* 2016; **151**:637–642.
37. Nastri CO, Lensen SF, Gibreel A, Raine-Fenning N, Ferriani RA, Bhattacharya S, Martins WP. Endometrial injury in women undergoing assisted reproductive techniques. *Cochrane Database Syst Rev* 2015(3):CD009517.
38. Nadeau-Vallee M, Obari D, Palacios J, Brien ME, Duval C, Chemtob S, Girard S. Sterile inflammation and pregnancy complications: a review. *Reproduction* 2016; **152**:R277–R292.
39. Pio R, Martinez A, Unsworth EJ, Kowalak JA, Bengoechea JA, Zipfel PF, Elsasser TH, Cuttitta F. Complement factor H is a serum-binding protein for adrenomedullin, and the resulting complex modulates the bioactivities of both partners. *J Biol Chem* 2001; **276**:12292–12300.
40. Parente R, Clark SJ, Inforzato A, Day AJ. Complement factor H in host defense and immune evasion. *Cell Mol Life Sci* 2017; **74**:1605–1624.
41. Girardi G, Yarilin D, Thurman JM, Holers VM, Salmon JE. Complement activation induces dysregulation of angiogenic factors and causes fetal rejection and growth restriction. *J Exp Med* 2006; **203**:2165–2175.
42. Huang J, Qin H, Yang Y, Chen X, Zhang J, Laird S, Wang CC, Chan TF, Li TC. A comparison of transcriptomic profiles in endometrium during window of implantation between women with unexplained recurrent implantation failure and recurrent miscarriage. *Reproduction* 2017; **153**:749–758.
43. Mor G, Cardenas I, Abrahams V, Guller S. Inflammation and pregnancy: the role of the immune system at the implantation site. *Ann N Y Acad Sci* 2011; **1221**:80–87.
44. Chen Q, Zhang Y, Elad D, Jaffa AJ, Cao Y, Ye X, Duan E. Navigating the site for embryo implantation: biomechanical and molecular regulation of intrauterine embryo distribution. *Mol Aspects Med* 2013; **34**:1024–1042.
45. Quinn CE, Detmar J, Casper RF. Pinopodes are present in Lif null and Hoxa10 null mice. *Fertil Steril* 2007; **88**:1021–1028.
46. Kabir-Salmani M, Nikzad H, Shiokawa S, Akimoto Y, Iwashita M. Secretory role for human uterodomes (pinopods): secretion of LIF. *Mol Hum Reprod* 2005; **11**:553–559.
47. Quinn C, Ryan E, Claessens EA, Greenblatt E, Hawrylyshyn P, Cruickshank B, Hannam T, Dunk C, Casper RF. The presence of pinopodes in the human endometrium does not delineate the implantation window. *Fertil Steril* 2007; **87**:1015–1021.
48. Adams SM, Gayer N, Hosie MJ, Murphy CR. Human uterodomes (pinopods) do not display pinocytotic function. *Hum Reprod* 2002; **17**:1980–1986.
49. Parr MB, Parr EL. Endocytosis in the uterine epithelium of the mouse. *J Reprod Fertil* 1977; **50**:151–153.
50. Cullinan-Bove K, Koos RD. Vascular endothelial growth factor/vascular permeability factor expression in the rat uterus: rapid stimulation by estrogen correlates with estrogen-induced increases in uterine capillary permeability and growth. *Endocrinology* 1993; **133**:829–837.
51. Jablonski EM, McConnell NA, Hughes FM, Jr, Huet-Hudson YM. Estrogen regulation of aquaporins in the mouse uterus: potential roles in uterine water movement. *Biol Reprod* 2003; **69**:1481–1487.
52. Richard C, Gao J, Brown N, Reese J. Aquaporin water channel genes are differentially expressed and regulated by ovarian steroids during the periimplantation period in the mouse. *Endocrinology* 2003; **144**:1533–1541.
53. Salleh N, Baines DL, Naftalin RJ, Milligan SR. The hormonal control of uterine luminal fluid secretion and absorption. *J Membr Biol* 2005; **206**:17–28.
54. Wetzel-Strong SE, Li M, Espenschied ST, Caron KM. Cohort of estrogen-induced microRNAs regulate adrenomedullin expression. *Am J Physiol Regul Integr Comp Physiol* 2016; **310**:R209–R216.
55. Watanabe H, Takahashi E, Kobayashi M, Goto M, Krust A, Chambon P, Iguchi T. The estrogen-responsive adrenomedullin and receptor-modifying protein 3 gene identified by DNA microarray analysis are directly regulated by estrogen receptor. *J Mol Endocrinol* 2006; **36**:81–89.
56. Laws MJ, Taylor RN, Sidell N, DeMayo FJ, Lydon JP, Gutstein DE, Bagchi MK, Bagchi IC. Gap junction communication between uterine stromal cells plays a critical role in pregnancy-associated neovascularization and embryo survival. *Development* 2008; **135**:2659–2668.
57. Penchalaneni J, Wimalawansa SJ, Yallampalli C. Adrenomedullin antagonist treatment during early gestation in rats causes fetoplacental growth restriction through apoptosis. *Biol Reprod* 2004; **71**:1475–1483.
58. Li L, Tang F, O WS. Preimplantation antagonism of adrenomedullin action compromises fetoplacental development and reduces litter size. *Theriogenology* 2012; **77**:1846–1853.
59. Li M, Schwerbrock NM, Lenhart PM, Fritz-Six KL, Kadmiel M, Christine KS, Kraus DM, Espenschied ST, Willcockson HH, Mack CP, Caron KM. Fetal-derived adrenomedullin mediates the innate immune milieu of the placenta. *J Clin Invest* 2013; **123**:2408–2420.
60. Matson BC, Corty RW, Karpinich NO, Murtha AP, Valdar W, Grotegut CA, Caron KM. Midregional pro-adrenomedullin plasma concentrations are blunted in severe preeclampsia. *Placenta* 2014; **35**:780–783.
61. Lenhart PM, Nguyen T, Wise A, Caron KM, Herring AH, Stuebe AM. Adrenomedullin signaling pathway polymorphisms and adverse pregnancy outcomes. *Am J Perinatol* 2014; **31**:327–334.